Author/s:
Akinoglu, EM;Song, J;Kinnear, C;Xue, Y;Zhang, H;Roberts, A;Köhler, J;Mulvaney, P

Title:
Concealed Structural Colors Uncovered by Light Scattering

Date:
2020-11-01

Citation:
Akinoglu, E. M., Song, J., Kinnear, C., Xue, Y., Zhang, H., Roberts, A., Köhler, J. & Mulvaney, P. (2020). Concealed Structural Colors Uncovered by Light Scattering. Advanced Optical Materials, 8 (22), https://doi.org/10.1002/adom.202001307.

Persistent Link:
https://hdl.handle.net/11343/284278

Concealed Structural Colours Uncovered by Light Scattering

Eser Metin Akinoglu, Jingchao Song, Calum Kinnear, Yafei Xue, Heyou Zhang, Ann Roberts, Jürgen Köhler, Paul Mulvaney*

Dr. Eser Metin Akinoglu, Mr. Heyou Zhang, Prof. Paul Mulvaney

ARC Centre of Excellence in Exciton Science, School of Chemistry, University of Melbourne, Parkville, VIC, 3010, Australia

Email: e.a@fu-berlin.de

Dr. Jingchao Song, Prof. Ann Roberts

ARC Centre of Excellence for Transformative Meta Optical Systems, School of Physics, University of Melbourne, Parkville, VIC, 3010, Australia

Dr. Calum Kinnear

CSIRO Manufacturing, Ian Wark Laboratories, Bayview Avenue, Clayton, Victoria 3168, Australia

Mr Yafei Xue

International Academy of Optoelectronics at Zhaoqing, South China Normal University, Zhaoqing, 526238 Guangdong, P. R. China

Prof. Jürgen Köhler

Spectroscopy of Soft Matter, University of Bayreuth, Universitätsstraße 30, 94557 Bayreuth, Germany

This is the author manuscript accepted for publication and has undergone full peer review but has not been through the copyediting, typesetting, pagination and proofreading process, which may lead to differences between this version and the Version of Record. Please cite this article as doi: 10.1002/adom.202001307.

Prof. Jürgen Köhler

Bavarian Polymer Institute, Universitätsstraße 30, 94557 Bayreuth, Germany

Prof. Jürgen Köhler

Bayreuth Institute of Macromolecular Research (BIMF), University of Bayreuth, Universitätsstraße 30, 94557 Bayreuth, Germany

Abstract

We demonstrate unusual structural colours in thin-film coatings due to a combination of optical interference and light scattering effects. These vivid colours are concealed under ambient illumination but can be observed when light is reflected from the film surface. We explore the origin of the effect computationally and show that, in thin-films of lossless dielectrics coated on near-perfect conductors, incident electromagnetic waves form standing waves. Electric field intensities at the thin film interfaces are maximized for wavelengths that fulfil destructive interference conditions, while nanoscale roughness can enhance scattering at these boundaries. The interplay of two factors yields vivid, thickness-dependent colours. This approach increases the repertoire of optical effects and perceived colours in thin coatings. When combined with traditional thin-film interference colours, we can generate dichromatic images with distinctly changing colours, which can function as a covert, optical security feature.

Introduction

Structural colours with a purely physical origin are an important phenomenon in nature.[1] A typical example of structural colour found in nature is provided by the blue wings of the Morpho Butterfly, which are a result of physical phenomena and not to blue pigments.[2] Because such vivid colours are typically not achievable with dyes or pigments, and because physical effects are dependent on precisely arranged material combinations on the nanometre and micron length scales, materials exhibiting structural colour have been used as security features on bank notes and sensitive documents, and have also gained much interest in the context of fundamental optics and for application in displays and sensors.[3] Structural colours are primarily due to diffraction and interference of light in periodic structures but light scattering, which has its origin in structural irregularities, is also important.[4] Traditional thin film interference is a phenomenon that gives soap bubbles and oil slicks on water their characteristic colours. Similarly, thin dielectric films on reflecting substrates such as thermally oxidized silicon, titanium and tungsten surfaces, and thin-films deposited by top-down methods can all exhibit strong

colours.[5] For instance, it is well known that a thin-film coating of Si_3N_4, which is a lossless dielectric, on a polished and reflecting silicon substrate exhibits a diverse range of thickness-dependent colours; however, the same Si_3N_4 film on a smooth aluminium substrate appears metallic. This is shown in Figure 1a, which presents photographs of both silicon surfaces (bottom) and aluminium surfaces (top) coated with Si_3N_4 thin-films of differing thickness. The classical explanation is, that the incident white light is reflected from the surface resulting in minima in the spectral response. For silicon, extinction of spectral regions renders the material coloured, such as magenta as shown in the schematic (Figure1b). However, aluminium is a nearly ideal electrical conductor with high reflection coefficient and therefore it evinces shallow interference minima without extinction of spectral regions, as shown schematically in Figure 1c. Hence, dielectric films on silicon and on aluminium do not exhibit the same optical effect. For aluminium there is only subtle colouration and these surfaces remain excellent mirrors with high durability (Figure 1a). In fact, dielectric coated aluminium mirrors are commonly employed as key components in telescopes and optical set-ups because aluminium is both cheaper and more robust than silver, while maintaining broadband reflection.[6] Here we report on a previously unrecognized curiosity – we observe angularly independent but thickness-dependent colours due to selectively scattered light from thin dielectric films on aluminium but not on silicon. Typical examples of this colour effect are shown in Figure 1d where the same samples as in Figure 1a are depicted. These show their scattering response (or diffuse reflection by deflecting white light off their surface) instead of their specular reflection. Schematically this is shown for silicon as an absence of radial scattering in Figure 1b and for aluminium as a radially diminishing green haze in Figure 1c. It is noteworthy, that the colour of the scattered light from the aluminium-based films is complementary to the colour observed in specular reflection from the silicon-based films for the same dielectric film thickness. These colours cannot be explained by classical interference phenomena alone. This optical effect has not been described previously and represents a new form of structural colour, which we explore through experiment, simulations and a theoretical framework. We find that these unexplored structural colours are due to a combination of both scattering and interference at the same time. Specifically, interference produces a maximum in the magnitude of the total field at the interface that leads to strong scattering associated with surface roughness at that boundary. Furthermore, these effects are hidden when viewing under regular, uncollimated, illumination but they are revealed by viewing the non-specular reflection of the samples. Finally, we utilize a partially aluminized silicon surface coated with a uniform dielectric film to exploit both effects. We demonstrate a

dichromatic image with distinctly changing colours when viewed in specular and non-specular reflection. The effect is schematically shown in Figure 1e, and photographs of a fabricated sample image depicting a kangaroo are shown in Figure 1f.

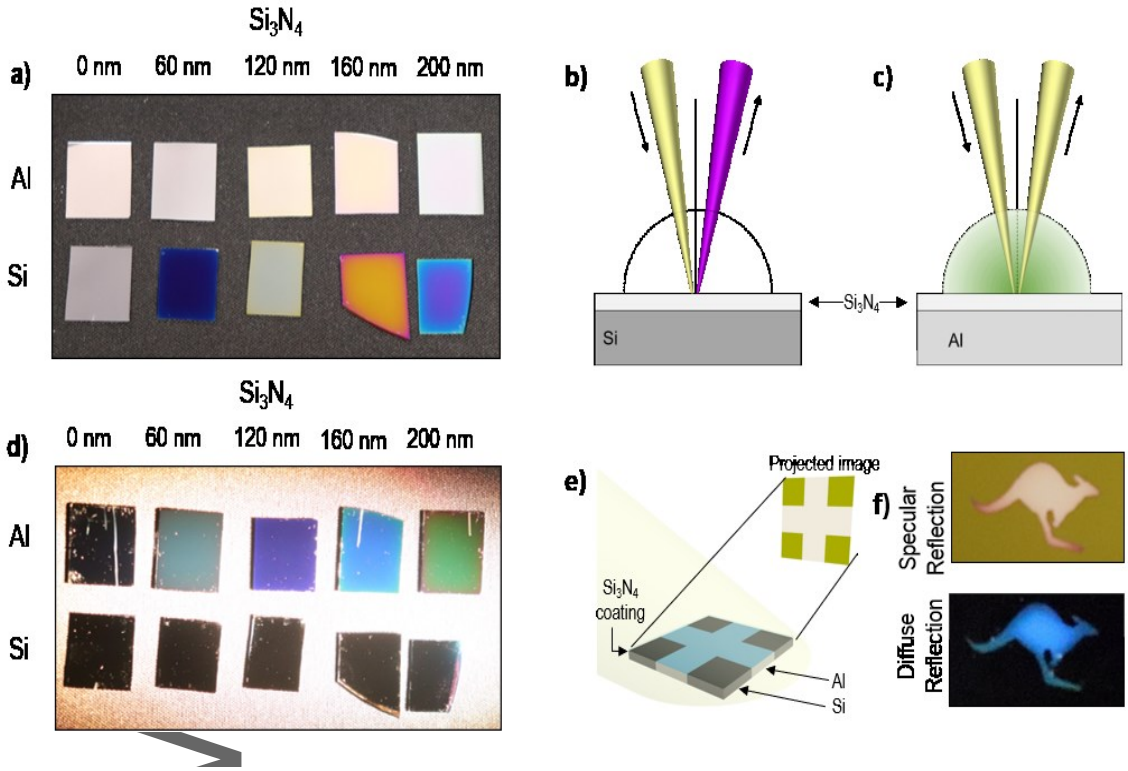

Figure 1. Overview of the effect. a) the colour of aluminium and silicon samples coated with different thicknesses of Si_3N_4 in reflection. The Si_3N_4 coated Si samples have distinct colours, whereas the bare Si and all Al based samples are near-ideal mirrors. b) is a schematic showing that interference from a silicon-based film results in an observable colour, here magenta, while no colour is observed for the aluminium-based films shown in c). d) the colour of the same samples as in a) when light is scattered off their surfaces. In this case the Si_3N_4 coated Al samples exhibit a distinct colour, whereas the bare Al and all-silicon based samples are black due to a lack of light scattering. The scattering from the aluminium-based films is schematically illustrated as a radially diminishing green haze in c) and is not present in b). Furthermore, the observed colours in b) and c) are complementary. Both effects can be combined to generate switchable dichromatic images schematically shown in e) and demonstrated in the form of a 160 nm Si_3N_4 coating on a 10 mm x 10 mm Kangaroo shaped Al film on Si in f). The sizes of the samples in a) and d) are approximately 15 mm x 15 mm.

Materials and Methods

Sample fabrication

Pieces of polished silicon wafers were cleaned by sonication in acetone, isopropyl alcohol, and Milli-Q water and dried with N_2 prior to use. For the metallic coating, 200 nm of aluminium was e-beam evaporated onto the cleaved silicon substrates using an Intlvac Nanochrome II evaporation system. Silicon nitride was then simultaneously deposited onto samples both with and without the metallic coating via plasma-enhanced chemical vapor deposition (PECVD) with an Oxford Instruments PLASMALAB 100 PECVD system. The thickness was determined by thin-film interferometry and by ellipsometry. The kangaroo motifs were fabricated by e-beam evaporation of aluminium onto a silicon wafer through a laser-etched polypropylene mask, followed by deposition of 160 nm of Si_3N_4. For the roughness dependent study, a 8 nm thick discontinuous layer of gold was evaporated onto the Si_3N_4 films as a shadow mask during reactive ion etching (RIE). An RIE system (Oxford Instruments PLASMALAB100 ICP380) was used to etch and generate surface roughness on the samples using a gas composition of O_2 (50 sccm), Ar (40 sccm), CHF_3 (30 sccm) and 1000 W forward power. Subsequently the Au etching mask was removed chemically with aqua regia, this was followed by rinsing with Milli-Q water and blow drying with N_2 gas.

Characterization

Optical constants (Figure S1) for the coatings were extracted via ellipsometry of the samples using a J.A Woollam M-2000DI spectroscopic ellipsometer at three different angles. The roughness of the samples was determined by atomic force microscopy using an Asylum Research MFP-3D-BIO AFM. Scanning electron microscopy (SEM) was performed with a ZEISS Sigma 500 scanning electron microscope. Total and diffuse reflection spectra were collected with a Perkin-Elmer LAMBDA 1050 UV/Vis Spectrophotometer using an integrating sphere. Variable angle measurements were performed with the centre mount accessory. The photograph in Figure 1a was taken at an angle of ~45^{o} from the surface normal in a well-illuminated room with ceiling lighting. Similarly, the photograph in Figure 1b was taken at approximately 45° from the surface normal while the samples were irradiated with a white flashlight at 45° angle from the surface normal and at a 90° angle from the camera so that specularly reflected light was not caputured by the camera. Furthermore the flashlight

was positioned closer to the samples than the camera to ensure that the camera did not capture light directly from the light source.

Simulations

The COMSOL Radio Frequency (RF) 2D model (electromagnetic Waves, Frequency Domain, (emw)) was used for all Finite Difference Time Domain (FDTD) simulations. The model used a 10 μm high and 1 μm wide unit cell with the dielectric film centred in the middle. Periodic boundary conditions were employed on the side boundaries. The top boundary of the cell was the input port for the wave excitation, whereas the bottom boundary was the output port. The optical constant for the materials were imported from ellipsometry measurements. The reflection coefficients were calculated via the two-port S-parameter model.

Results and Discussion

Photographs of silicon and aluminium surfaces with Si_3N_4 coatings of varying thickness are shown in Figure 1. In general, the colour of these samples is governed by their specular reflectance (Figure 1a). All Al based metals and bare Si are good mirrors with faint colouration. In contrast, the Si_3N_4 coated Si samples exhibit distinct colours, which are dependent on the Si_3N_4 film thickness. However, the colour of all samples is changed when white light is reflected from their surface but only the scattered light is seen (Figure 1d). In the absence of specular reflection, only scattered light, i.e. diffuse reflection, is observed. Here, the Si_3N_4 coated Al samples exhibit a pronounced colour, whereas the bare Al and all Si based samples appear black. Additional examples for colours observed on Si_3N_4 coated Al are shown in Figure S2. Specular and diffuse reflectance spectra reveal that interference plays a key role. For all Si_3N_4 coated Al films, the specular reflectance spectra are dominated by a large overall reflectance typical for aluminium with shallow minima (Figure 2a). Hence, only very narrow band widths of the visible spectrum are partially filtered out, rendering the surface slightly metallic in appearance. In contrast, all Si_3N_4 coated Si surfaces exhibit weaker overall specular reflectance (Figure 2b) typical of polished Si wafers. Here, the minima of the thin film interference approach zero intensity corresponding to selective elimination of complete spectral regions, which results in typical thin-film interference colours (Figure 1a). The observed specular reflectance $R_S = r^2$ of these dielectric coated reflective substrates can be understood in terms of the Fresnel equation

$$r = \frac{r_{12} + r_{23} e^{-2i\delta}}{1 + r_{12} r_{23} e^{-2i\delta}} \quad (1)$$

where δ is the phase shift and r_{12} and r_{23} are the Fresnel amplitude reflectance coefficients for the air-Si_3N_4 and the Si_3N_4-substrate interface respectively.[5] Simulated spectra based on this eq. [1] (Figure S3) reproduce the measurements and confirm this classical interpretation. Here, the minima are associated with destructive interference and occur for $\delta = (2m\text{-}1)\pi$ where the integer $m \geq 1$ indicates the interference order. This condition is met for $\delta = 2\pi nd/\lambda \cos(\theta)$ where n is the refractive index of the insulator medium, *d is* the insulator film thickness, θ is the angle of incidence, and λ is the wavelength of incident light, in vacuum. The angular dependence implies a spectral shift to meet the destructive interference condition, and hence a change in colour.

Angle dependent, specular reflectance spectra collected from both samples (Figure S4) show the expected blue shift of the destructive interference minima for increasing the angle θ. However, it is evident that th spectral shift as a function of θ is small and therefore results only in minor variations in the perceived visible colour. This is due to the small phase accumulation of light traversing through very thin films.[7]

The diffuse reflectance from the Si_3N_4 coated Al films shows that their observed iridescent colour is correlated to their thin film interference signature, observed in specular reflectance. In particular, these thin film stacks exhibit a maximum in diffuse reflectance for those values of λ where destructive interference minima are observed in specular reflectance (Figure 2c). In contrast, the Si_3N_4 coated Si surfaces only show negligible diffuse reflectance intensities and these are two orders of magnitude lower than their Al based counterparts (Figure 2d). Hence, they

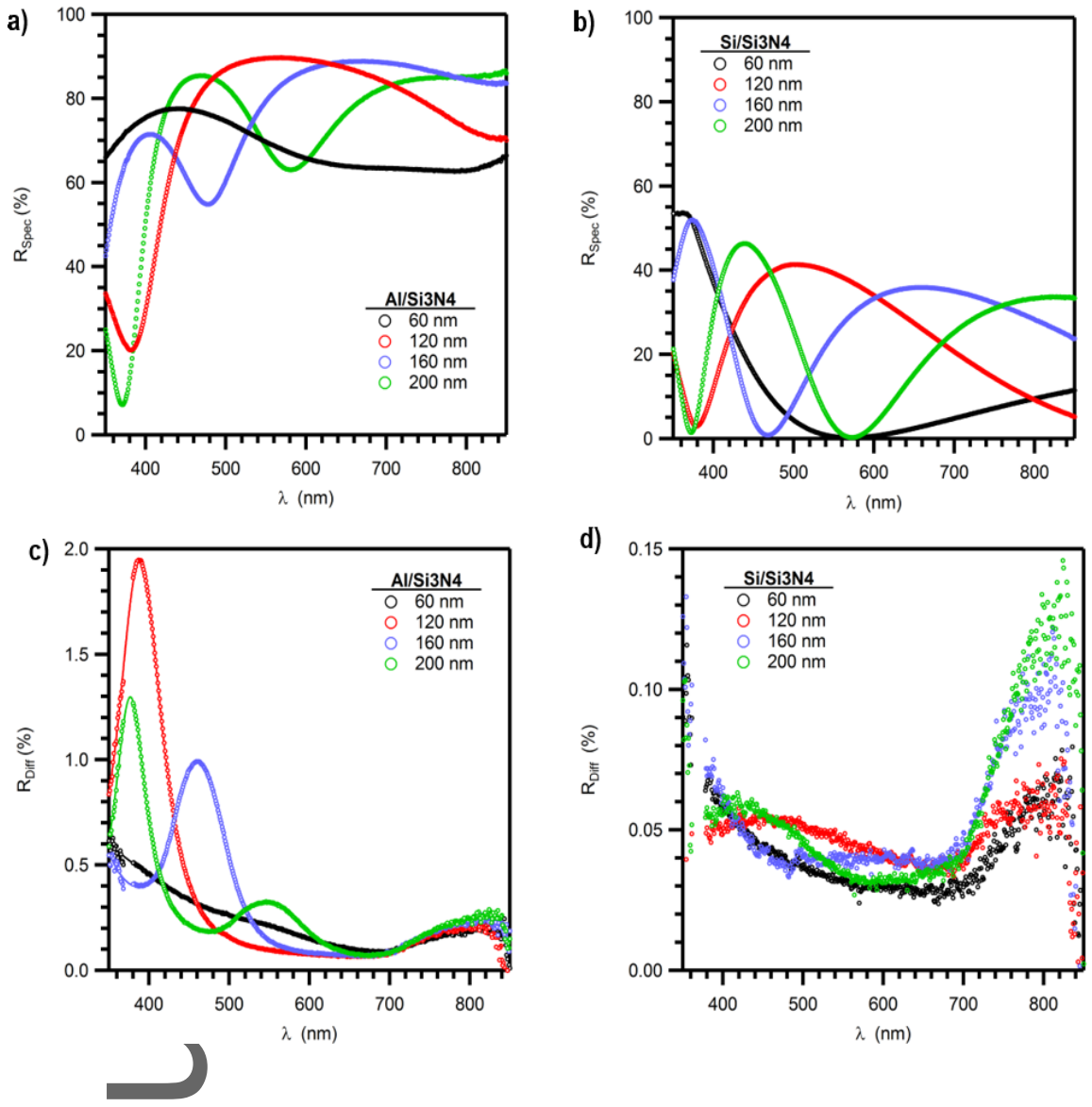

Figure 2. Optical response of thin film coatings. The specular reflection spectra of a) Si_3N_4 coated Al samples and b) Si_3N_4 coated Si samples. On a silicon surface, total extinction of some spectral regions occurs whereas a high overall reflectance on aluminium is preserved.The diffuse reflection spectra of c) Si_3N_4 coated Al samples and d) Si_3N_4 coated Si samples. On silicon no significant scattering is measured, while on aluminium surfaces, scattering maxima spectrally coincide with reflection minima. All Si_3N_4 thicknesses are indicated in the insets.

are perceived to be black when white light is reflected from their surfaces. It is important to note, that for diffuse reflectance R_D, i.e. scattering, the Fresnel equation does not hold and the above correlation between maxima in R_D and minima in R_S is not obvious. Generally, light scattering from interference coatings is determined by a complex mixture of factors including the roughness of all interfaces, the field distribution in the coating, and structural defects.[8,9]. The influence of the latter can be seen on the samples in Figure 1d in the form of bright spots or lines from particles or scratches. Light scattered in this way can be explained with geometrical optics and is not wavelength selective. Roughness induced scattering of multilayer coatings has a general $1/\lambda^4$ dependence and explains the increase in the background scattering towards the blue,[9] but cannot explain the dielectric film thickness dependent maxima in R_D. We note that cross-correlation between the roughness of the interfaces can be a determining factor for the angular scattering distribution and the coherent scattering associated with it.[10–12] Typically, this results in a subtle increase in the scattering intensities for certain solid

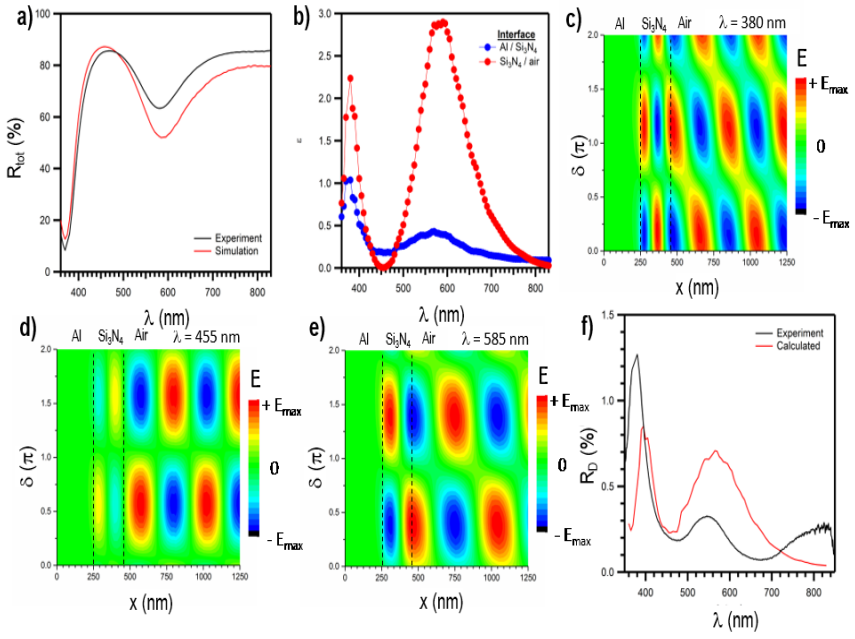

Figure 3. Electric field intensities on Al substrates modelled for a planar aluminum sample coated with a 200 nm thick Si_3N_4 film. a) Measured and simulated total reflection R_T. b) Calculated illumination function ε at the thin-film interfaces. Maxima in ε follow minima in R_T. c) Spatial electric field amplitude distribution for the first interference minimum at λ = 380 nm. d) Spatial electric field amplitude distribution for the first interference maximum at λ = 455 nm. e) Spatial electric field amplitude distribution for the second interference minimum at λ = 585 nm. The magnitude of the electric fields is colour coded: green represents E = 0 while the red and blue regions represent the positive (E >0) and negative (E <0) amplitudes of the plane wave respectively. The y-axis is tthe phase delay δ of the incident plane wave from 0 to 2π. This corresponds to a full period and represents the temporal evolution of the electric field intensities. The thin film interfaces are indicated with black dashed lines. The Si_3N_4-air interface coincides with an anti-node of a standing wave for destructive interference and with a node for constructive interference. f) shows the experimentally determined and calculated R_D.

angles, an effect that cannot be seen on these samples with the naked eye. The magnitude of the surface roughness induced light scattering for normal incidence can be estimated from

$$R_D = R_T\left(1 - e^{-\left(\frac{4\pi n\sigma}{\lambda}\right)^2}\right) \quad (2)$$

using scalar scattering theory. Here σ is the rms value of the surface roughness and R_T the total reflectance with $R_T=R_D+R_S$.[13] Atomic force microscopy images (Figure S5) reveal a factor of four increase in σ for the Al surfaces compared to the Si surfaces (Figure S6). Furthermore, only a minor roughness variation with increasing Si_3N_4 film thickness is observed, i.e. there is a minor increase in roughening on Si substrates but a slight decrease on Al substrates. A comparison of Figure 1 and Figure 2 immediately reveals, that roughness by itself

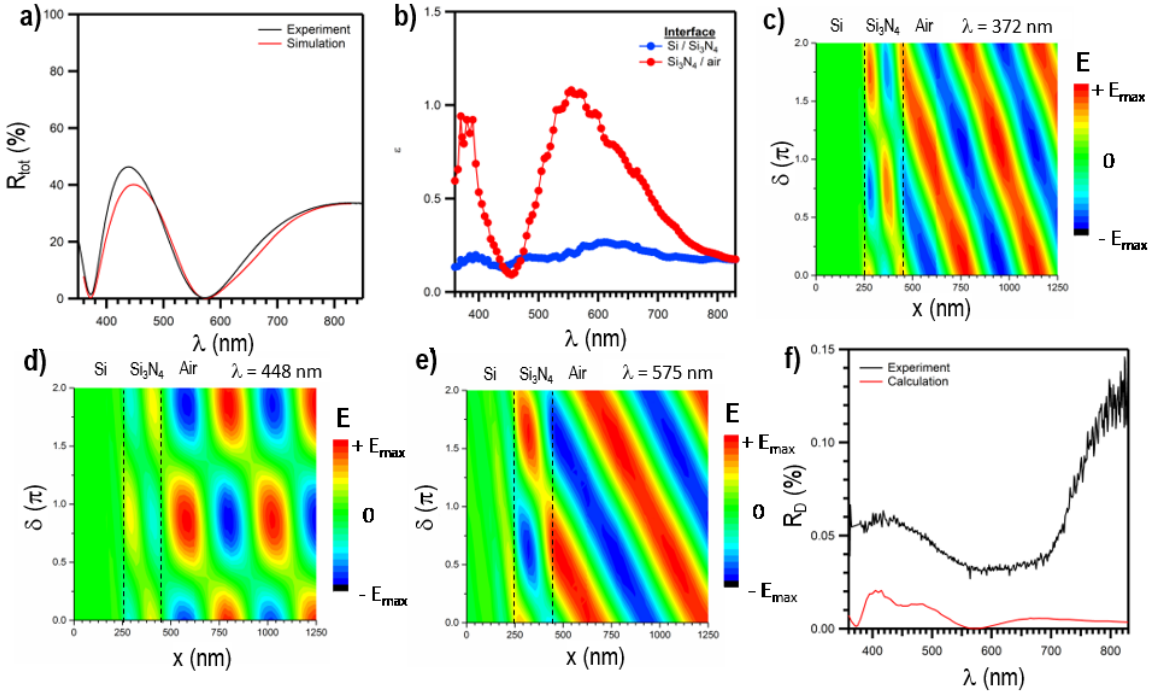

Figure 4. Electric field intensities on Si based samples modelled for a planar Si sample coated with a 200 nm thick Si_3N_4 film. a) Measured and simulated total reflection R_T. b) Calculated illumination function ε at the thin-film interfaces. Maxima in ε follow minima in R_T. c) Spatial electric field amplitude distribution for the first interference minimum at λ = 372 nm. d) Spatial electric field amplitude distribution for the first interference maximum at λ = 448 nm. e) Spatial electric field amplitude distribution for the second interference minimum at λ = 575 nm. The magnitude of the electric fields is colour coded with green representing E = 0 while the red and blue regions represent the positive (E >0) and negative (E <0) amplitudes of the plane wave respectively. The y-axis is the phase delay δ of the incident plane wave from 0 to 2π. This corresponds to a full period and represents the temporal evolution of the electric field intensities. The thin film interfaces are indicated with black dashed lines. For destructive interference travelling waves and energy dissipation into the substrate are observed, whereas a partial standing wave with its anti-nodes at the thin film interfaces is seen for constructive interference. f) shows the experimentally determined and calculated values of R_D.

cannot be the determining factor for the strong scattering off the Si_3N_4 coatings on Al, because (i) both bare Al and Si exhibit negligible diffuse reflection, and (ii) an interpretation purely based on scalar scattering theory would imply that the lineshape of the diffuse reflectance spectra should follow the spectra of specular reflection without inversion of the maxima and minima. However, light scattering also scales with $R_D \sim \langle E^2 \rangle$, where $\langle E^2 \rangle$ is the time average of the squared electric field.[14–19]. In general, $\langle E^2 \rangle$ will be greatly affected by interference phenomena. FDTD simulations are used to investigate the electric field distributions in a 200 nm thick Si_3N_4 coating on both Al (Figure 3) and Si (Figure 4) substrates. The experimental (black) and simulated (red) total reflection for a 200 nm Si_3N_4 coating on Al substrates are shown in Figure 3a. To match the experiment, the simulation assumes 204 nm Si_3N_4 thickness, which is well within the error of the experimental thickness measurement. $\langle E^2 \rangle$ is accounted for by the illumination function

$$\varepsilon(\lambda, x) = \frac{\langle E^2 \rangle}{\langle E_0^2 \rangle} \tag{3}$$

with incident electric field $\mathbf{E_0}$.[15] Figure 3b shows $\varepsilon(\lambda)$ at the Al-Si_3N_4 (blue) and Si_3N_4-air (red) interfaces, and illustrates that at both interfaces the electric fields will be at a maximum when the destructive interference condition is met, i.e. the minima of $R_{tot}(\lambda)$ coincide with the maxima of $\varepsilon(\lambda)$. To illustrate the electric field distribution in space, their amplitudes are mapped for the two cases of destructive interference at λ = 380 nm (Figure 3c) and λ = 585 nm (Figure 3e), and for the case of constructive interference at λ = 455 nm (Figure 3d). Here the x-axis slices through all interfaces of the thin film stack along the substrate normal, i.e. the aluminium-Si_3N_4 interface at x = 250 nm and the Si_3N_4-air interface at x = 454 nm indicated by black dashed lines. The incident light is modelled as a plane wave linearly polarized perpendicular to the substrate normal and the magnitude of its associated electric fields is colour coded with green representing E = 0 while red and blue represent the positive (E >0) and negative (E <0) amplitudes. The y-axis represents a variation of the phase delay δ of the incident plane wave from 0 to 2π. This corresponds to a full period equal to the temporal evolution of the electric field intensities. It is evident that in each case a standing wave is formed where the electric field abruptly vanishes at the aluminium- Si_3N_4 interface with negligible penetration of the field into the substrate. This is a consequence of the excellent electrical conductivity of Al. Furthermore, it is important to note that the Si_3N_4-air interface coincides with an anti-node of this standing wave for destructive interference (λ = 380 nm and λ =

585 nm) but coincides with a node (E = 0) for constructive interference (λ = 455 nm). To account for both the scattering due to surface roughness, and due to $\langle E^2 \rangle$ enhancement, a modulation of the scalar scattering theory solution (Eq. 2) by ε(λ) is permitted, where both interfaces are weighted equally.

$$R_D = R_T\left[\left\{\frac{1}{2}\left(1 - e^{-\left(\frac{4\pi n_{air}\sigma}{\lambda}\right)^2}\right)\varepsilon\left(\lambda, x_{f/air}\right)\right\} + \left\{\frac{1}{2}\left(1 - e^{-\left(\frac{4\pi n_f\sigma}{\lambda}\right)^2}\right)\varepsilon\left(\lambda, x_{s/f}\right)\right\}\right] \quad (4)$$

Here, the first term accounts for the thin film-air interface with the wavelength dependent illumination function $\varepsilon(\lambda, x_{f/air})$ and the refractive index of air n_{air}. The second term accounts for the substrate-film interface with $\varepsilon(\lambda, x_{s/f})$ and the refractive index of the film n_f. Putting in the experimentally determined values for R_T and σ = *3.15 nm*, and the simulated values for ε, we obtain reasonable agreement with the observed diffuse reflectance as shown in Figure 3f. Hence, the origin of the vivid colours observed on Al substrates is due to electric field enhanced scattering at the interfaces. Similar considerations were applied to the case of a 200 nm Si_3N_4 coating on Si substrate and the results are shown in Figure 4. The experimental (black) and simulated (red) values of R_T are shown in Figure 4a. To match the experiment, the simulation assumes 213 nm Si_3N_4 thickness, which is within the error of the experimental thickness measurement. Plots of ε(λ) at the Si-Si_3N_4 (blue) and the Si_3N_4-air (red) interfaces are presented in Figure 4b. In general the value of ε is smaller on Si substrates than on Al substrates. Furthermore, peaks and troughs in ε do not correlate directly with interference phenomena at the substrate-film interface. The illustrated electric field distributions in space in the case of destructive interference at λ = 372 nm (Figure 4c) and λ = 575 nm (Figure 4e) show typical travelling wave character with energy dissipation into the substrate (R_T = 0). In the case of constructive interference (λ = 575 nm), a partially travelling and partially standing wave is formed (Figure 4d). Eq. (4) is used to calculate R_D from R_T and σ = *1.02 nm*, and the simulated values for ε. Reasonable agreement between the measured and calculated R_D is observed as seen in Figure 4f. Evidently, the electric field enhancement and the smaller value of σ result in only marginal light scattering and hence the black appearance of the the Si based samples.

Eq. (4) implies that the scattered light intensity is strongly dependent on the surface roughness σ of the two interfaces. Conversely the colour can be tuned if the surface roughness can be controlled and varied. However, a fundamental implication of this equation is that with increasing σ the local fields $\langle E^2 \rangle$ diminish due to

broadening so only small values σ should be considered. The dependence of R_D on σ as per Eq. (4) for an aluminium supported 200 nm Si_3N_4 coating is shown in Figure 5. Two separate cases were considered. The results of a variation in the roughness at the aluminium- Si_3N_4 interface $\sigma_{Al/Si3N4}$ from 1 nm to 6 nm with a constant value of $\sigma_{Si3N4/air} = 3.15\ nm$ is shown in Figure 5a, while the effects of a variation in the roughness at the Si_3N_4-air interface $\sigma_{Si3N4/air}$ from 1 nm to 6 nm with a constant value of $\sigma_{Al/Si3N4} = 3.15\ nm$ is shown in Figure 5b. In both cases an increase in σ leads to an increase in R_D. Furthermore, an increase in $\sigma_{Al/Si3N4}$ leads to a stronger increase in the 2nd order peak compared to the 1st order peak. The opposite behaviour can be observed for an increase in $\sigma_{Si3N4/air}$, where the 1st order peak shows a stronger increase than the 2nd order peak. To verify this predicted behaviour and to verify that Eq. (4) holds, we studied the evolution of R_D as we deliberately roughened the Si_3N_4-air interface of an aluminium supported 200 nm Si_3N_4 thin film. To this end, we have evaporated 8 nm Au onto the sample surface to obtain a dense distribution of gold nanoparticles (Figure S7). For such a small Au deposition thickness, the gold particles act as the nucleation sites from which a continuous Au film forms for larger deposition thicknesses. Subsequently, these Au particles were used as an etching mask to induce anisotropy during reactive ion etching of the Si_3N_4 film. The Au particles shield parts of the Si_3N_4 surface from the reactive ion flux. After the etching process, the Au particles were removed completely with aqua regia to obtain the pristine roughened Si_3N_4 surfaces. This process increased the root mean squared surface roughness from approximately 2.5 nm to 3.0 nm. Unfortunately, because the roughness is determined from AFM topography measurements, and the scanning probe tip radius is ~7nm, a more precise value is not feasible. The total reflection R_T spectra for a series of increasingly roughened samples is shown in Figure 5c. Because the etching also thins the Si_3N_4 film, a blue-shift is observed. Furthermore, because $R_D \propto R_T$ from Eq. (4), the 1st order minimum intensity remains approximately constant, whereas the 2nd order minimum intensity substantially decreases. Hence, a further increase in etching to further roughen the surface is limited by the onset of the 1st order minimum intensity decrease. The corresponding diffuse reflection R_D spectra (Figure 5d) demonstrate that the 1st order maximum intensity increases with surface roughening in qualitative agreement with Eq. (4). The 2nd order maximum decreases in intensity, which can be accounted for by the decreasing value of R_T. Overall, the experimental evidence supports the semi-quantitative predictions of Eq. (4).

The fundamental requirement for this effect is that the electric field forms a node at the interface between the substrate and the thin dielectric film in order to maximize the intensity of $\varepsilon(\lambda)$. This condition is well met by excellent conductors such as aluminium and silver and is partially met for copper and gold films, where there are negligible optical absorption losses. On the other hand, the dielectric thin film coating should be colourless to observe the effect.

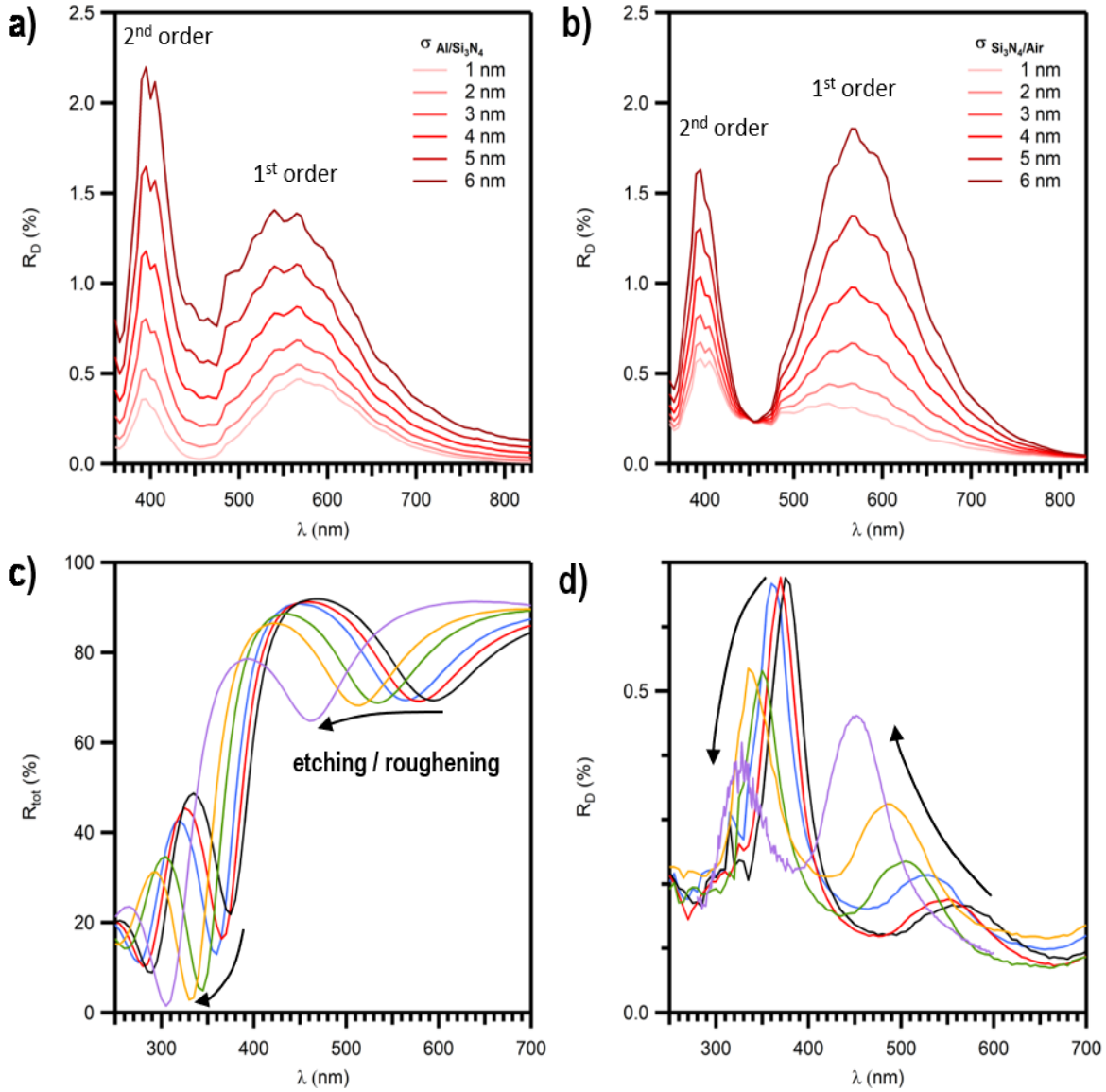

Figure 5. The effect of the roughness predicted by Eq. (4) compared to experiment for a Aluminum supported 200 nm Si_3N_4 thin film. a) shows the predicted diffuse reflection for varying $\sigma_{Al/Si3N4}$ calculated from the respective experimental total reflection and Eq. (4) and $\sigma_{Si3N4/air}$ = 3.15. b) shows the predicted diffuse reflection for varying $\sigma_{Si3N4/air}$ calculated from the respective experimental total reflection and Eq. (4) and $\sigma_{Al/Si3N4}$ = 3.15. c) shows the total reflection of a Aluminum supported 200 nm Si_3N_4 thin films that were subject to increasing etching/roughening as indicated by the black arrow. d) shows the corresponding diffuse reflection spectra.

Conclusions

In conclusion, the above results demonstrate that surface scattering from dielectric-coated, near-ideal conductors provide a useful lever for tuning structural colours in thin films. They may also be used to generate dichromatic images for aesthetic and security features. We have demonstrated that such non-intuitive structural colours in thin-film coatings result from interference mediated light scattering. Specular and diffuse reflectance spectra show reverse spectral minima and maxima. While thin-film interference and the Fresnel formalism account for the specular response, the perceived diffuse reflectance does not have a trivial origin. Computational analysis reveals strong spectral electric field variations at the coating interfaces when the latter is situated on nearly ideally conducting substrates due to the formation of standing waves. In particular, the electric fields are at a maximum at their anti-nodes, which are superimposed on destructive interference conditions present at the dielectric-air interface. In turn, this condition produces a modulation of the interfacial scattering. The effects can nonetheless be described by scalar scattering theory and this enables us to calculate the diffuse reflectance from the specular reflection, the electric field intensity analysis and surface roughness measurements. We have combined traditional thin-film interference colours with these new, concealed structural colours to fabricate dichromatic images with switchable colour as a potential new class of optical security feature. These effects could be further enhanced by incorporation of fluorescent dyes or excitonic materials to modulate the perceived colour.

Conflict of Interest

The authors declare no financial/commercial Conflict of Interest.

Acknowledgements

The research leading to these results has been funded by the Australian Government through the Australian Research Council Grant CE170100026 and the Guangdong Innovative and Entrepreneurial Team Program 2016ZT06C517. E.M.A. acknowledges funding by the Alexander von Humboldt Foundation through a Feodor Lynen Research Fellowship. Financial support by a Wilsmore fellowship granted by the University of Melbourne, as well as support by the Melbourne-Bayreuth Colloid/Polymer Network financed by the DAAD is gratefully acknowledged by J.K. This work was performed in part at the Melbourne Centre for Nanofabrication (MCN) in the Victorian Node of the Australian National Fabrication Facility (ANFF). J.S. acknowledges the technical support provided by Dan Smith from MCN.

References

[1] S. Kinoshita, S. Yoshioka, *Chemphyschem a European journal of chemical physics and physical chemistry* **2005**, *6*, 1442.
[2] P. Vukusic, J. R. Sambles, C. R. Lawrence, *Nature* **2000**, *404*, 457.
[3] A. E. Goodling, S. Nagelberg, B. Kaehr, C. H. Meredith, S. I. Cheon, A. P. Saunders, M. Kolle, L. D. Zarzar, *Nature* **2019**, *566*, 523.
[4] S. Kinoshita, S. Yoshioka, J. Miyazaki, *Rep. Prog. Phys.* **2008**, *71*, 76401.
[5] M. Born, E. Wolf, *Principles of optics: Electromagnetic theory of propagation, interference and diffraction of light*, Pergamon Press, Oxford **1993**.
[6] D. D. Allred, L. E. Tilahun, J. G. Richardson, R. S. Turley (Eds.), *Expanding the Far UV Range of Aluminum-Coated Mirrors for Space-Based Observations to Reflect Hydrogen Lyman Lines via Fluoride Multilayers*, Optical Society of America **2019**.
[7] M. A. Kats, R. Blanchard, P. Genevet, F. Capasso, *Nature materials* **2013**, *12*, 20.
[8] J. M. Bennett, *Thin Solid Films* **1985**, *123*, 27.
[9] S. Schröder, M. Trost, M. Garrick, A. Duparré, X. Cheng, J. Zhang, Z. Wang, *Thin Solid Films* **2015**, *592*, 248.
[10] S. Schröder, D. Unglaub, M. Trost, X. Cheng, J. Zhang, A. Duparré, *Applied optics* **2014**, *53*, A35-41.
[11] T. Nordam, P. A. Letnes, I. Simonsen, A. A. Maradudin, *Optics express* **2012**, *20*, 11336.
[12] R. O. Prum, R. H. Torres, S. Williamson, J. Dyck, *Nature* **1998**, *396*, 28.
[13] J. M. Elson, J. M. Bennett, *Opt. Eng* **1979**, *18*.
[14] A. Roos, D. Rönnow, *Applied optics* **1994**, *33*, 7908.
[15] A. Roos, M. Bergkvist, C. G. Ribbing, *Applied optics* **1989**, *28*, 1360.
[16] M. Bergkvist, A. Roos, C. G. Ribbing, J. M. Bennett, L. Mattsson, *Applied optics* **1989**, *28*, 3902.
[17] A. Roos, M. Bergkvist, C. G. Ribbing, *Applied optics* **1988**, *27*, 4314.
[18] A. Roos, M. Bergkvist, C.-G. Ribbing, *Thin Solid Films* **1985**, *125*, 221.
[19] M. Bergkvist, C.-G. Ribbing, A. Roos, P. Temple, *Physics Letters A* **1986**, *116*, 343.

Concealed structural colours are uncovered and used to prepare dichromatic images. A unique optical effect combining the physics of optical interference and light scattering is discovered on near-perfect conductors coated with thin dielectric films. Standing waves inside the thin-films yield frequency selective electric field maximization at the film interface, which results in frequency selective enhanced scattering manifesting as vivid colours.